Effects of mutation on the amyloidogenic propensity of apolipoprotein C-II$_{60–70}$ peptide†

Nevena Todorova,[a] Andrew Hung,[a] Simon M. Maaser,[b] Michael D. W. Griffin,[b] John Karas,[c] Geoffrey J. Howlett[b] and Irene Yarovsky*[a]

Received 21st April 2010, Accepted 10th September 2010
DOI: 10.1039/c0cp00299b

Using experimental and computational methods we identified the effects of mutation on the structure and dynamics of the amyloidogenic peptide apoC-II(60–70), in monomeric and oligomeric states. Methionine (Met60) substitutions to hydrophilic Gln, hydrophobic Val, and methionine sulfoxide residues were investigated and the results compared with observations of fibril formation by the wild-type, Met60Gln, Met60Val, and oxidised Met60 (oxi-Met) apoC-II(60–70) peptides. ThT fluorescence measurements showed fibril formation by all peptides, however with different kinetics. The wild-type and Met60Val peptides formed fibrils fastest, while oxi-Met and Met60Gln peptides exhibited significantly longer lag phases. Molecular dynamics simulations showed that the mutated monomers exhibited structural features consistent with fibril-forming propensity, such as β-hairpin conformation and a hydrophobic core. However, important differences to the wild-type were also noted, such as increased structural flexibility (oxi-Met and Met60Gln systems) and a broader distribution of the aromatic angle orientation, which could contribute to the different fibrillation kinetics observed in these peptides. Our results also showed that the critical nucleus size for fibril formation by apoC-II(60–70) may not be very large, since tetrameric oligomers in anti-parallel configuration were very stable within the 100 ns of simulations. The single-point mutations Met60Val and Met60Gln had no significant effect on the structural stability of the tetramer. The rate of fibril formation by apoC-II(60–70) peptides was generally much faster compared to longer apoC-II(56–76) peptides. Also, the effects of amino acid modifications on the kinetics of peptide fibril formation differ from the effects observed for apoC-II(56–76) and full-length apoC-II, suggesting that additional mechanisms are involved in fibril formation by mature apoC-II.

Introduction

Misfolded proteins can self-associate to form amorphous aggregates or elongated fibre structures, known as amyloid fibrils. The deposition of amyloid fibrils in the human body has been linked to many debilitating diseases, such as Alzheimer's, Parkinson's, diabetes type 2 and atherosclerosis, thus making this field of research important and urgent. While the general cross-β structure of amyloid fibrils has been defined, the initial misfolding of the protein and subsequent self-association into the fibrils are poorly understood. Recent studies suggest that the cytotoxic and disease forming species are the prefibrillar intermediates.[1–4] A possible therapeutic strategy against amyloid diseases could be the application of specific mutant or truncated variants that prevent the nucleation of the fibrils or assist in their dissociation. Detailed knowledge of the structure of the respective species at different stages of formation is essential in order to design such compounds. Hydrophobic effects are considered to be the main driving force determining aggregation and fibrillation. In the early stages of Aβ-assembly, hydrophobic and bend-like structures are required to produce amyloid fibrils.[5,6] Residue substitution methods have been applied in many studies of amyloidogenic proteins to determine specific amino-acid contributions to fibril formation, stability and dissociation. Specifically, the effects of oxidation are of interest due to their reversibility and promising inhibitory effects.[7,8]

Human apolipoprotein (apo) C-II readily aggregates into twisted ribbon-like fibrils at physiological pH and without prolonged agitation.[9] ApoC-II and several other apolipoproteins have been identified in atherosclerotic plaques *in vivo*[10] and it is found colocalised in human coronary artery plaques with serum amyloid P, a non-fibrillar marker of amyloid deposits.[11] The effects of single residue mutations on the fibril forming propensities of native apoC-II and smaller apoC-II derived peptides have been investigated experimentally.[12–14] Full-length apoC-II protein contains two Met residues, one found at the beginning of the amino acid sequence (position 9) and the other in the fibril forming core (position 60). Studies of the

[a] *Health Innovations Research Institute, School of Applied Sciences, RMIT University, Melbourne, VIC, Australia. E-mail: irene.yarovsky@rmit.edu.au; Fax: +61 3 9925 5290; Tel: +61 3 9925 2571*
[b] *Biochemistry and Molecular Biology and Bio21 Molecular Science and Biotechnology Institute, The University of Melbourne, Melbourne, VIC, Australia*
[c] *Bio21 Molecular Science and Biotechnology Institute, The University of Melbourne, Melbourne, VIC, Australia*

† Electronic supplementary information (ESI) available: Secondary structure evolution plots from additional simulations and cartoon representation of structural models not shown in the main text of the article. See DOI: 10.1039/c0cp00299b

effect of oxidation and mutation of these residues demonstrated significant inhibition of apoC-II aggregation when Met60 was oxidised, while a lesser effect was seen upon oxidation of Met9.[12] Mutation studies of these residues showed that when Met60 was replaced by Val the protein formed fibrils with a similar rate and morphology as the wild-type. Mutation of Met60 to Gln also leads to the formation of fibrils, however much higher protein concentration was required.[12] Short peptide fragments composed of apoC-II residues 60 to 70 have been proposed as the driving fibril forming sequence in apoC-II.[15] A recent experimental and computational study performed by Hung and co-workers investigated the influences of phospholipids, methionine oxidation and acidic pH on the structure and dynamics of the isolated apoC-II(60–70) peptide.[13] Under fibril-favouring conditions (neutral and low pH) the peptide preferentially adopts structures similar in shape to a β-hairpin, while under fibril-disruptive conditions (lipid-rich and oxidised Met) significantly different structures were obtained. The formation of β-hairpin structures in relatively short amyloidogenic peptides has been observed in several peptides, such as LSFD,[16] amyloid-β(25–35)[17] and in an 11-residue fragment of β2-microglobulin.[18] The development of β-hairpin structures in amyloidogenic peptides suggests this type of conformation to be a state a peptide monomer exhibits prior to association, indicating that this structure is favourable for peptide aggregation. In a more recent study, experimental and computational techniques were implemented to explore the effect of oxidation and mutation of Met60 to Val and Gln on the stability of apoC-II(56–76) peptide.[14] Wild-type apoC-II(56–76) and apoC-II(56–76)Met60Gln peptides readily assembled into fibrils with similar lag phase, whereas the apoC-II(56–76) with oxidised Met formed fibrils with much slower kinetics. The slowest to form fibrils was the apoC-II(56–76)Met60Val peptide, which exhibited totally different aggregation kinetics compared to the full-length apoC-II with the same mutation. Legge and co-workers observed that the aggregation behaviour of the apoC-II(56–76) peptide system is different to that of the full length protein system, suggesting that the mechanism of fibril formation may also be different.[14]

In this paper we extended the previous work[13,14] by performing *in vitro* measurements of fibril formation and molecular dynamics simulations on the shorter amyloidogenic apoC-II(60–70) peptide. Recent findings showing differences in the fibrillation kinetics between the full-length and derivative apoC-II(56–76)[14] peptides were extended to a comparison with the structural and kinetics studies of apoC-II(60–70). Single-point residue substitutions were performed at Met60 to hydrophobic Val (Met60Val) and hydrophilic Gln (Met60Gln) and the results were compared with the behaviour of the wild-type and oxidised apoC-II(60–70) peptides.[13] The Gln amino acid was chosen because of the similar hydrophilicity to the oxidised Met, while mutation of Met to Val enabled the effects of hydrophobic substitution on peptide structure to be examined. Using fully solvated molecular dynamics simulations, we aimed to identify the conformational preferences in monomeric and oligomeric apoC-II(60–70) species that could be responsible for the experimentally observed differences in aggregation kinetics and provide important insight into the possible features that influence the peptide's fibril-forming or inhibiting propensities. In addition to the studies of monomeric apoC-II(60–70) peptide, we also report molecular dynamics simulations of apoC-II(60–70) oligomeric assemblies of various sizes and arrangements, namely dimeric, trimeric and tetrameric single β-sheet formations, in parallel and anti-parallel strand orientations with different terminal states, charged and neutral. The effects of oxidation of Met60, and Met60Val and Met60Gln mutation on the structure and dynamics of the most stable oligomer were also studied.

Results and discussions

Fibril formation by peptide derivatives

ApoC-II(60–70) is a small peptide which has the ability to independently form amyloid fibrils, suggesting that this region is involved in driving fibril formation by the full-length protein. It is the smallest and therefore the most convenient system for studying the effects of modifications at position 60 and relating these results to effects observed within the full-length protein. ThT fluorescence experiments were performed on wild-type and mutated apoC-II(60–70) peptides (Fig. 1). The results show fibril formation by all peptides, however with different kinetics. The wild-type and Met60Val peptides formed fibrils faster, while oxi-Met and Met60Gln peptides exhibited significantly longer lag phases. Upon incubation of the wild-type apoC-II(60–70) peptide with a refolding buffer, a rapid increase in ThT fluorescence is seen up until 6 hours after which ThT fluorescence declined. The development of ThT fluorescence on incubation of the Met60Val derivative showed a sharp increase between 4 and 7 hours, followed by a slower rate of fluorescence increase up until 72 hours. For both the methionine oxidised (oxi-Met) and glutamine (Met60Gln) mutated peptides an extended initial lag phase of approximately 72 hours (3 days) was visible before any significant increase in ThT fluorescence. CD spectra reveal that all peptides adopted predominantly random coil structure when freshly diluted from the stock solutions (not shown) and acquired secondary structure over the time course of fibril formation, consistent with our previous observations of the longer 56–76 peptide.[14] These data indicate that any differences between the solution structures of each peptide variant were subtle, and that all peptides shifted from dynamic, coil-like structures in solution to stable and ordered conformations in the fibril.

TEM images of fibrils formed by each of the peptide derivatives show differences in their gross morphology (Fig. 1d). The wild-type peptide fibrils appeared as aggregated, straight, flat sheet-like structures with no twists or bends. The fibrils were of relatively short length with an average width of approximately 20 nm. In comparison, the oxi-Met and Met60Val apoC-II(60–70) fibrils were generally many microns long with a width of approximately 10–15 nm. These fibrils also appear to readily intertwine creating a larger, branching network of fibrils. The Met60Gln peptide fibrils displayed a twisted morphology similar to that observed for the oxi-Met and Met60Val peptide derivatives. However, these fibrils were

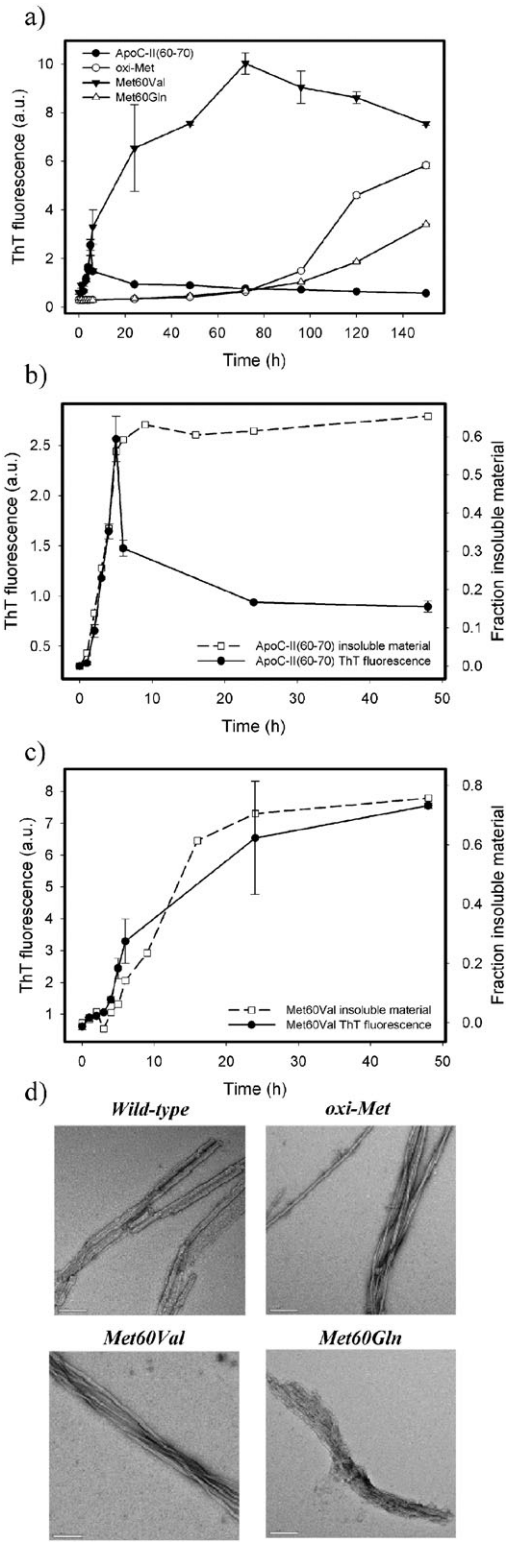

Fig. 1 The effect of mutations at position 60 on the fibrillisation of apoC-II(60–70). (a) Thioflavin T fluorescence time course data for the native peptide, oxi-Met, Met60Val and Met60Gln. (b) For the wild-type peptide and (c) Met60Val the fraction of insoluble material over time is superposed on the ThT fluorescence data. (d) Transmission electron microscopy images of apoC-II(60–70) peptide derivatives (0.1 mg ml^{-1} final concentration) incubated at 0.3 mg ml^{-1} in 100 mM sodium phosphate, pH 7.4 for 150 hours prior to observation. Scale bar is 100 nm. All peptides were incubated at 0.3 mg ml^{-1} (240 μM).

sparser and considerably thinner with a width of only 5 nm. Fig. 1a–c show that ThT fluorescence intensity in the presence of each of these fibril types was different, despite a uniform peptide concentration. We propose that this was due to differential binding of ThT to the fibril surface, caused by the observed morphological and structural differences. We have previously shown that full length apoC-II can form two fibril morphologies with different underlying molecular structures, and that these induce significantly different ThT fluorescence intensities.[19]

The accumulation of insoluble material during the course of fibril formation was followed for the wild-type and Met60Val peptides (Fig. 1b and 1c). These data overlaid closely with the ThT fluorescence development for these peptides, suggesting that fibril formation constituted the primary aggregation process and that little or no peptide was being lost in 'off-pathway' aggregation processes. This assertion is also supported by the absence of significant amounts of amorphous aggregates observed on each of the TEM grids. The level of insoluble material for the wild-type peptide remains relatively constant after around 6 hours while the ThT fluorescence measured for this peptide drops after this time. This reduction in ThT fluorescence is most likely due to the secondary aggregation of fibrils to form fibril clumps, thereby reducing the ability of ThT to bind to the fibrils.

Comparing the results seen here for the apoC-II(60–70) peptides with those from our previous experiments on apoC-II(56–76),[14] we note that fibril formation occurs more slowly for the apoC-II(56–76) peptide when compared to apoC-II(60–70) peptide, distinguishable by the 48–72 h (2–3 days) lag phase, which may be attributed to the larger size of apoC-II(56–76). From the previous studies of full-length apoC-II,[12] apoC-II(56–76)[14] and the studies presented here, it is evident that additional mechanisms are involved in the fibrillation process of different sized peptides which contribute to the different fibrillation behavior and kinetics.

Molecular dynamics simulations

Structural evolution analysis of monomeric apoC-II(60–70). Molecular dynamics (MD) simulations described in the following sections have been used to provide insight into the experimentally observed differences in peptide aggregation behaviour. The secondary structure dynamics reveal details of the conformational changes experienced by the protein over the entire simulation period. This is especially useful because the peptides under investigation differ by a single residue only, so the secondary structure evolution makes it possible to examine the effect of each mutation. The secondary structure was classified using the algorithm STRIDE which utilises hydrogen bond energy and mainchain dihedral angles in addition to bond distances.[20] The structural evolution plots of the wild-type and oxidised apoC-II(60–70)[13] are shown together with those for the mutated apoC-II(60–70) systems in Fig. 2. To examine the most frequently occurring conformations in each simulation, an RMSD based clustering method was utilised with an RMSD cutoff of 0.15 nm applied to the whole molecule. The two most populated structures and their corresponding population are shown together with the secondary structure plots in Fig. 2.

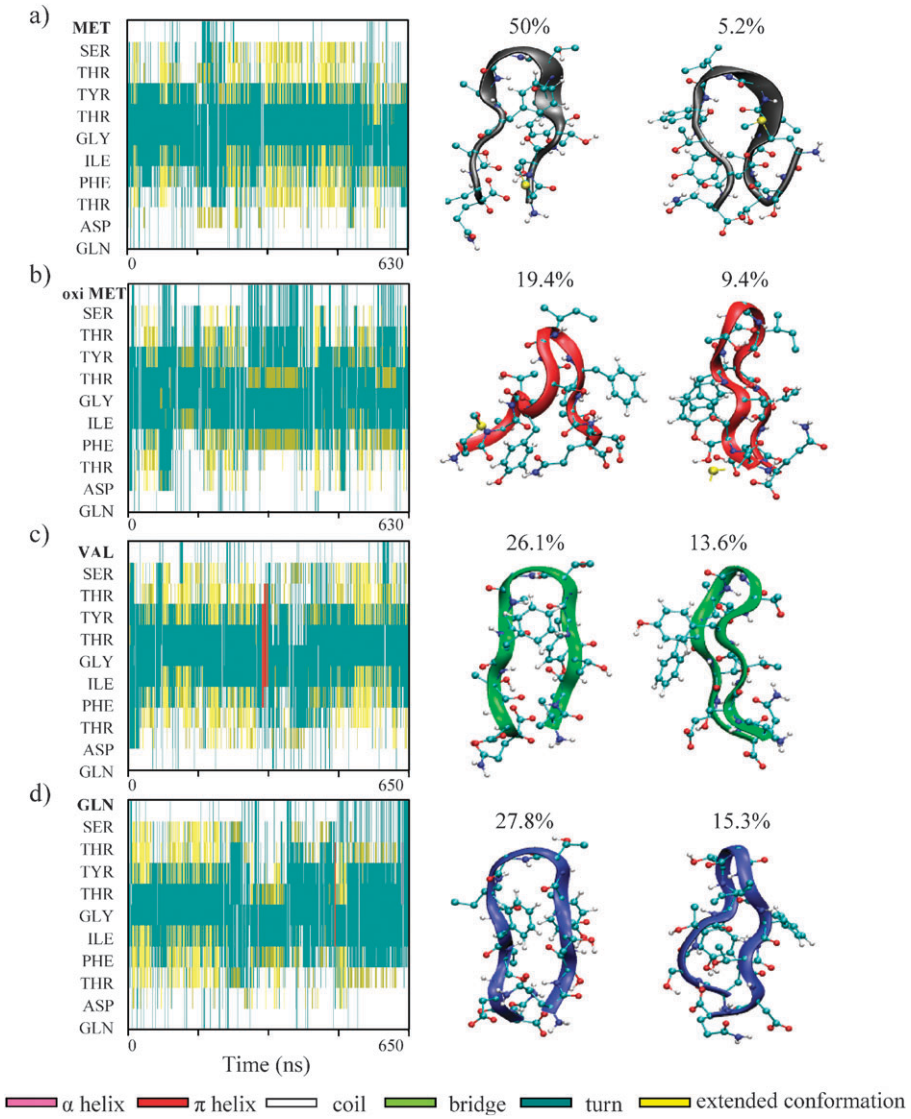

Fig. 2 Secondary structure evolution plot for each mutation of apoC-II(60–70) peptide; (a) wild-type; (b) oxi-Met; (c) Met60Val; (d) Met60Gln. The secondary structure colour codes: magenta—α helix, red—π helix, cyan—turn, white—coil, yellow—extended conformation and green—hydrogen bridge. The first two most populated structures obtained by cluster analysis are shown.

The wild-type apoC-II(60–70) peptide exhibited stable conformations with well defined structural features (Fig. 2a). In particular, the β-hairpin motif was identified throughout the simulation. The β-hairpin structure was defined by two strands, Ser61-Tyr63 (strand 1) and Phe67-Asp69 (strand 2), that are adjacent in primary structure and form a loop in an anti-parallel arrangement (where the N-terminus of one strand is adjacent to the C-terminus of the other strand). The anti-parallel strands were linked by a short turn region composed of three residues, Thr64, Gly65 and Ile66. A similar turn structure was identified in the MD study of the apoC-II derived peptide comprising residues 56 to 76.[21] Legge *et al.* postulated that this turn region is an important feature of the nucleation stage of fibril formation since it enables the formation of a stable hydrophobic core. As seen from our fibrillisation measurements (Fig. 1), and also recent experimental data,[13] the wild-type apoC-II(60–70) peptides readily aggregate into fibrils, so the turn structure observed in the dynamics of this peptide is consistent with the conditions required for aggregation. The cluster analysis of the wild-type apoC-II(60–70) peptide identified 1259 distinct clusters. Close inspection of the representative structure from the most populated cluster shows the presence of a β-hairpin conformation (Fig. 2a). The most populated cluster contains 50% of the structures generated by the simulations, highlighting the stability of this type of structure, compared to only 5.2% of the second most populated cluster.

Inspection of the 630 ns simulation of the oxidised Met (oxi-Met) apoC-II(60–70) peptide showed several important changes in the secondary structure (Fig. 2b). A stable core turn region formed between residues Tyr63 and Ile66 in the initial ~250 ns of simulation, followed by a shift of the turn to residues Thr64-Phe67. This structural element was supported by the formation of a hydrogen-bond bridge between these residues. In contrast, the three residues of each peptide terminus fluctuated between a turn and coil conformations,

indicating no significant interactions between these regions of the two strands. Overall, oxi-Met exhibited higher structural flexibility compared to the wild-type apoC-II(60–70) peptide, with less hydrogen bonding and electrostatic interactions between strands 1 and 2. However the core turn region between Thr64-Ile66 was well maintained. The greater flexibility observed in the secondary structure analysis of the oxi-Met simulation was reflected by the increased number of clusters classified, 1417, where the most populated cluster contained 19.4% of the structures used in the clustering analysis. A representative structure of this cluster (Fig. 2b) has a core turn region between residues Thr64 and Ile66. The termini are well separated from each other, with the sulfoxide of the Met oriented towards the solvent. The second most populated cluster (9.4%) is in the form of a β-hairpin with the two aromatic rings being solvent exposed in a π-stack orientation. This arrangement of the rings possibly has a stabilising effect on the hairpin conformation and can potentially facilitate the formation of fibrils,[13] however, the increased flexibility of the peptide could contribute to slower fibril formation identified experimentally (Fig. 1).

Distinct structural features were observed in the Met60Val mutated system compared to the oxi-Met, with the mutated structures showing greater similarity in conformation to the wild-type peptide. Throughout the simulation the Met60Val mutated peptide exhibited the β-hairpin conformation, where the core turn region between residues Thr64 and Ile66 was maintained by the electrostatic interactions between the two β-stranded chains, represented by yellow in Fig. 2c. After ~320 ns of simulation the peptide displayed a turn conformation followed by a partial fold into a π-helix. This conformation lasted for ~17 ns, after which the peptide folded back into a β-hairpin that was retained for the rest of the simulation. These observations highlight the peptide's distinct preference for the β-hairpin conformation, in par with the fibrillation kinetics (Fig. 1) and simulated similar type conformations of the wild-type peptide.

Increased variation in the secondary structure was seen in the Met60Gln system compared to the Met60Val mutation (Fig. 2d). A stable β-hairpin structure was observed for the initial ~250 ns, with a core turn region between Thr64 and Gly65. This was followed by a shift of the core turn to residues Gly65-Ile66. Further flexibility was observed through an extension of the central turn of the peptide to the region between residues Tyr63 and Phe67. This β-hairpin conformation was stabilised in the last ~100 ns of the simulation by hydrogen bonds between the two Thr residues at positions 62 and 68, respectively. A short-lived π-helix fold was noted when there was a reduction in interaction between the terminal residues of the peptide and an extension in the overall structure was observed. This type of development was also identified in the simulations using Charmm27 force field on the same point mutations of the apoC-II(56–76) peptide,[14,21] suggesting the π-helix to be a genuine feature of these mutations rather than a force field artifact. Interestingly, no π-helix formation was observed in the oxidised Met simulation, possibly due to the well maintained central hydrophobic core restricting the extension of the peptide.

The clustering analysis of the Met60Val and Met60Gln simulations showed similar results with respect to the structures sampled and their relative population, highlighting the structural resemblance of these peptides. Altogether, 1460 and 1358 clusters were classified, with the most populated clusters of the peptides containing 26.1% and 27.8% of the structures, respectively. These structures exhibited the β-hairpin motif with a core turn region between residues Thr64 and Ile66. Interestingly, the most populated clusters of the Met60Val and Met60Gln mutated peptides exhibited features very similar to the most populated cluster obtained from the wild-type apoC-II(60–70) simulation. The higher number of clusters determined for the mutated systems compared to the wild-type peptide reflects higher conformational flexibility of these systems which was also observed in the secondary structure analysis.

In the second most highly populated cluster of Met60Val and Met60Gln simulations, the structures exhibit slightly distorted hairpin conformations, mostly differing in the arrangement of the aromatic rings. The significance of the relative orientation of the aromatic side-chains in individual peptides is discussed later.

Even though some increased flexibility was observed in the Met60Val and Met60Gln mutated peptides compared to the wild-type, overall these systems maintained the β-hairpin motif throughout the simulations, with the hydrophobic core stabilised by hydrogen bonding and electrostatic interactions. It can be suggested that the preservation of the hydrophobic core may provide the necessary conditions for aggregation observed by our fluorescence experiments (Fig. 1). Interestingly, the formation of stable β-hairpin structure was recently observed in a fibril-forming 12 amino acid sequence denoted as LSFD.[16] The core hairpin turn in this work consisted of a Gly-Ala sequence. We note that in the simulated apoC-II(60–70) peptides, the location of the Gly is central in the three residue turn region (Thr64, Gly65, Ile66). This suggests a nascent formation of turns and bends at the Gly residue, leading to an overall U-shaped topology (strand-turn-strand) of the backbone which facilitates the formation of intramolecular sheets. However, the increased flexibility and reduced hydrogen bonding and electrostatic interactions between the termini regions observed in the oxidised Met simulation, may contribute to the slower fibril formation seen from the fibril formation kinetics experiments.

Aromatic side-chain orientation. The role of the aromatic rings in fibril formation was shown to be significant, specifically in relation to their presence in fibril forming regions and their contribution to fibril stability.[22] Site-directed modification performed on short amyloidogenic fragments revealed that aromatic residues play a crucial part in the fibrillation process.[23] In the case of the IAPP motif mutation of Phe to Ala there was a significant reduction in the peptides potential for fibril formation.[24] The presence of two aromatic rings (Tyr63 and Phe67) in the apoC-II(60–70) peptide suggests their possible role in aggregation propensity and kinetics. The orientation of their side-chains is of significant interest, as distinct differences were recently identified between fibril forming and inhibiting conditions.[13]

In order to reveal the effect of mutation on the aromatic side-chain orientation the relative position of the aromatic side-chains with respect to the peptide backbone structure was determined. We calculated the average angle between the Cα–Cγ vector of Tyr63 and the Cα–Cγ vector of Phe67, during the equilibrium part of the simulation of the Met60Val and Met60Gln peptides. Angles of less than 90° indicate that the two side-chains lie on the same "face-side" of the peptide structure, while angles greater than 90° indicate that the side-chains are on the opposite faces of the hairpin. Results from our recent work[13] showed that the peptide under fibril-favouring conditions adopts structures where Tyr63 and Phe67 prefer the opposite sides of the hairpin structure, whereas the structures obtained under fibril-inhibiting conditions have the aromatic rings on the same side of the hairpin. The histograms and representative structures obtained from the Met60Val and Met60Gln simulations are shown in Fig. 3. The angles determined for oxi-Met and wild-type apoC-II(60–70) from our previous work[13] are also presented for comparison.

The angles adopted by the aromatic side-chains of Met60Val and Met60Gln peptides lie approximately between 130° and 150°, similar to the wild-type peptide, with the majority of structures containing the aromatic rings located on opposite faces of the hairpin structure. The similar orientation of the Tyr63 and Phe67 side-chains between the mutated and native peptides suggests favourable arrangement for fibril formation. However, the broader distribution of angles for the mutated system is consistent with the differences seen in fibrillation kinetics for these peptides (Fig. 1).

Solvation properties. The solvation properties and conformational changes due to the peptide–solvent interactions are important, as shown in a recent study by Wei and Shea on the effect of solvents on the conformations of the Aβ peptide.[17] This study highlighted the influence of solvent on the conformational states of amyloidogenic peptides that may result in fibril formation or inhibition. Their simulations revealed that the Aβ(25–35) peptide preferentially populated a helical structure in apolar organic solvent (postulated to be fibril inhibiting), while in pure water, the peptide adopted collapsed coil and β-hairpin conformations which did form fibrils. Fernandez and Scheraga[25] have noted that proteins that aggregate readily tend to have a significant number of backbone H-bond donors/acceptors exposed to the solvent, available for protein–protein interaction. Therefore quantifying the exposure to solvent is important for understanding of peptide association tendencies.

The average solvent accessible surface area (SASA) and average number of water molecules found in the first hydration shell of each peptide were calculated and are presented in Fig. 4. The averages were determined from the structures contained in the most populated cluster of each simulation. The SASA was calculated for each system using a probe radius of 1.4 Å (water) and Lennard-Jones hard-shell radii for each atom to define the surface. The number of water molecules present in the first hydration shell, that is within a 3 Å distance of each residue, was also calculated.

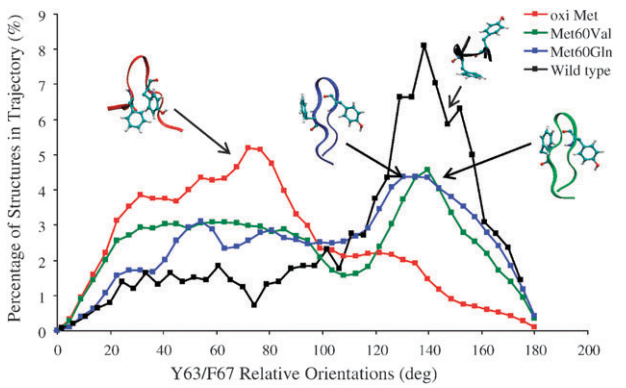

Fig. 3 Histograms of Tyr63 ring orientation with respect to Phe67 (*x*-axis), obtained from total simulated trajectories for oxidised methionine (red),[13] Met60Val (green), Met60Gln (blue) and wild-type (black) peptides. *y*-Axis indicates the percentage of structures for a specific orientation angle range exhibited during the trajectory. Forty bins were used over the range 0–180°. Each data point represents the percentage (%) of structures with orientation angles between *x* and *x* + 4.5°. Angle < 90° indicates both rings are on one side of the hairpin, while >90° indicates rings exist on opposite sides. Structures illustrating the relative ring orientations are represented in insets.

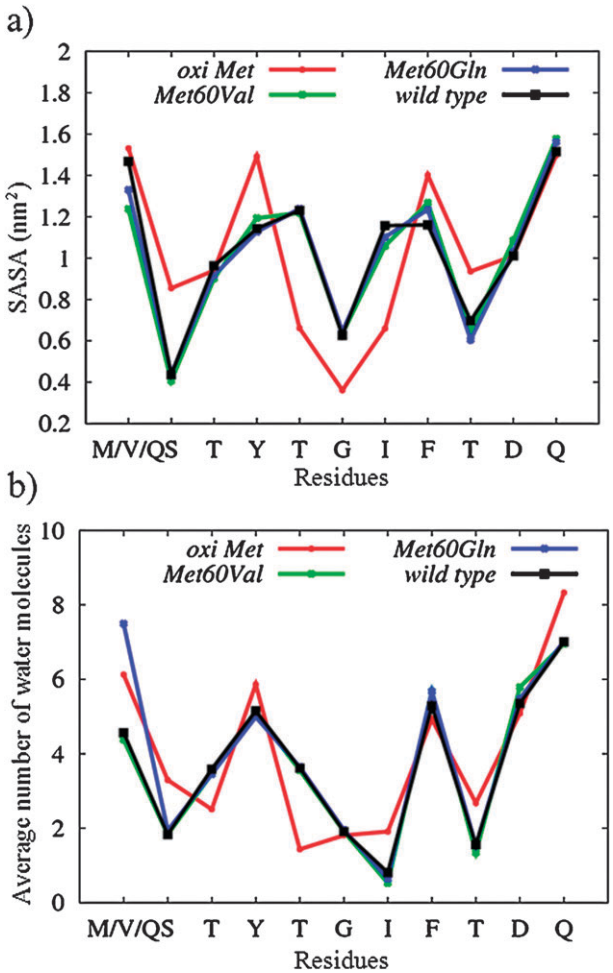

Fig. 4 Average values calculated per residue over the structures contained in the most populated cluster of the oxidised methionine (red), Met60Val (green), Met60Gln (blue) and wild-type (black) simulation. (a) Solvent accessible surface area (nm²); (b) the average number of water molecules within a 3 Å shell of each residue.

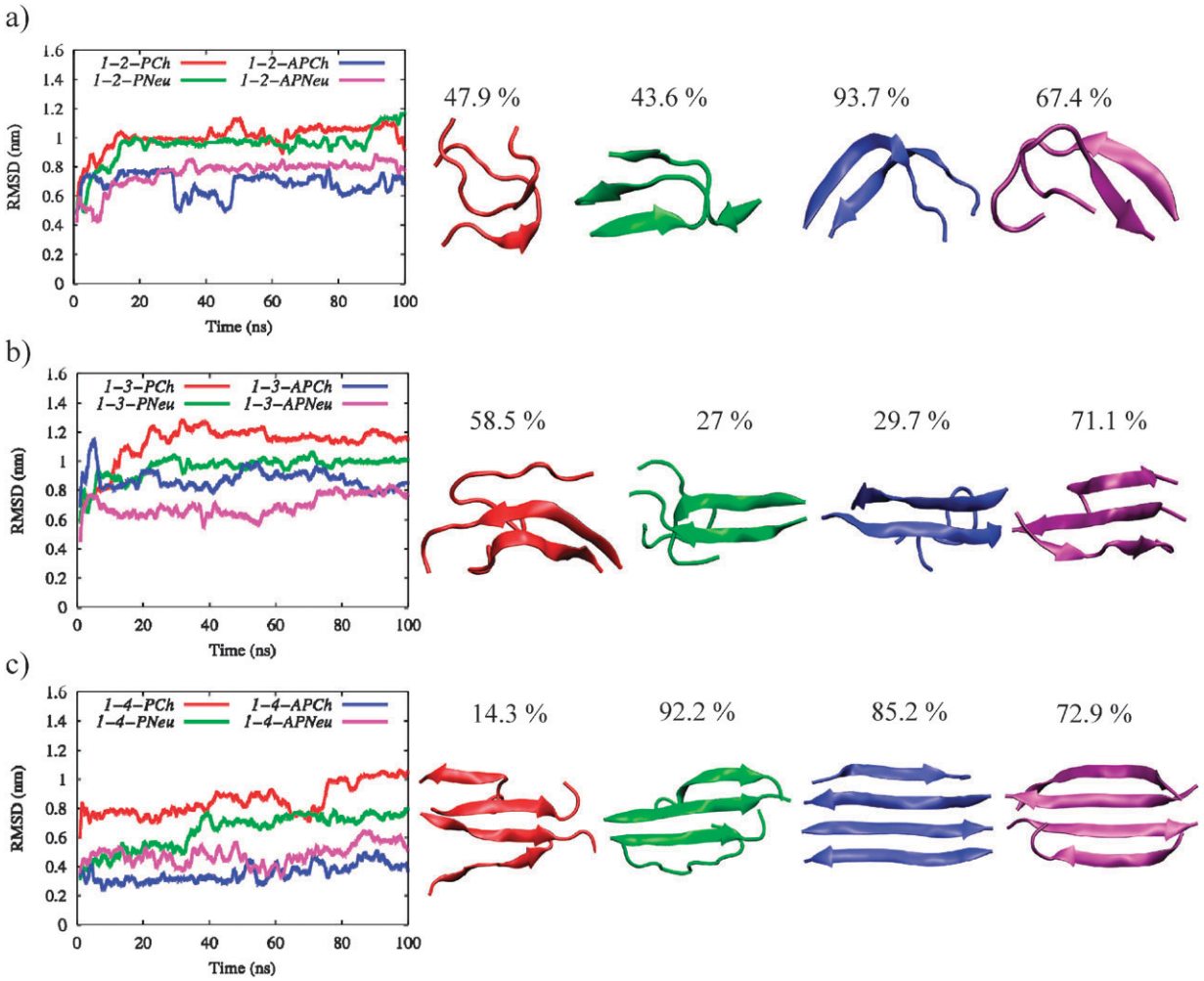

Fig. 5 Root mean square deviation (RMSD) plots of the trajectories of apoC-II(60–70), (a) dimer, (b) trimer and (c) tetramer oligomers. The structures of the most populated clusters of every system and their population are also presented.

Interestingly, there is only a small difference in the total SASA of the structures within the most populated clusters of each system, wild-type = 11.41 nm^2, oxi-Met = 11.34 nm^2 and Met60Val and Met60Gln = 11.23 nm^2, respectively. However, the SASA per residue for the oxi-Met is very different to the SASA of the wild-type, Met60Val and Met60Gln peptides.

In the oxidised system, the SASA per residue of the oxi-Met60 and Gln70 residues are almost equal in value, while Gln70 has on average two more water molecules within a 3 Å shell compared to oxi-Met (Fig. 4b). This is a result of the side-chain interaction of oxi-Met with the Ser61 and Thr62, yet Gln70 is exposed for full solvation. The destabilising effect of oxidation of Met60 on the interaction between the strands contributes to a higher SASA in this region compared to the wild-type and mutant systems where attractive interaction between the strands minimises their exposure to the solvent. In contrast, the SASA of the core turn region (Thr64-Ile66) of the oxidised peptide is lower compared to the mutated peptides, which in turn have similar SASA to the wild-type apoC-II(60–70). The hydrophobic core between residues Thr64, Gly65 and Ile66 is retained within the structures of the most populated cluster of the oxidised system, which results in the observed decrease in SASA of these residues and reduced number of surrounding water molecules (Fig. 4).

Our simulations indicate that in the wild-type, Met60Val and Met60Gln peptides the residues, comprising the β-turn region, Thr64, Gly65 and Ile66, are more exposed to water than those of the oxidised peptide (Fig. 4). This suggests that the β-turn in Met60Val and Met60Gln may be responsible for initiating aggregation. Furthermore, the similarities seen in Fig. 4 for Val and Gln mutated fragments with the fibril-forming wild-type peptide[13] suggest that aggregation propensity could be a nascent property for these apoC-II(60–70) peptides, as indeed was confirmed experimentally (Fig. 1).

The low solvent exposure of the hydrophobic core region (Thr64, Gly65, Ile66) in the oxidised system may reduce the interactions with "like" peptides and contribute to the slower fibril formation observed by our ThT fluorescence experiments. In contrast, in the wild-type and mutant systems, the exposure of the hydrophobic region is higher, so the interactions between "hydrophobic patches" from different peptides can drive their aggregation and could possibly form fibrils faster. It is important to emphasise that we performed SASA calculations on the structures contained within the most

populated cluster, thus the described differences in solvation between the oxidised peptide and the wild-type, Met60Val and Met60Gln mutated peptides are due to their preferred structural features. However, the second most populated cluster of the oxidised peptide contained β-hairpin conformations, with similar solvent exposure to the other peptides. This suggests that although the most populated structure of the oxidised peptide exhibits different structural features compared to the other systems, the development of β-hairpin structures is also possible. This can create the necessary fibril favouring conditions in the oxidised peptide system, albeit to less extent than in the other peptide systems, thus explaining the experimentally observed fibril forming behaviour (Fig. 1).

Wild-type apoC-II(60–70) oligomeric stability: RMSD and clustering analysis. In the second part of this study, we examined the conformational stability of pre-formed oligomers of the wild-type apoC-II(60–70) peptide. In particular, the most favorable strand orientation and the effects of the termini charges were of interest. The stability of each oligomer was monitored by calculating the root mean square deviation (RMSD) of the backbone over the entire trajectory of 100 ns. RMSD analysis is a widely used measure for the stability of protein and oligomer structures.[26–28] In order to determine the most populated structure of every oligomer, clustering analysis was performed using every second frame of the trajectory (12 500 frames). The RMSD plot together with the most populated structures and their population for the dimer, trimer and tetramer of apoC-II(60–70) are presented in Fig. 5.

The highest RMSD values were exhibited by the dimers in parallel arrangement, 1-2-PCh and 1-2-PNeu having an average RMSD of 1.16 nm and 1.08 nm, respectively. The anti-parallel dimers exhibited lower RMSD values, with 1-2-APCh and 1-2-APNeu having an average RMSD of 0.83 nm and 0.91 nm, respectively. The significant change in the parallel structure compared to anti-parallel dimers was demonstrated by the lower population of structures in the most stable parallel clusters, 47.9% and 43.6%, *versus* 93.7% and 67.4% for the anti-parallel clusters. These results indicated that the parallel arrangement of apoC-II(60–70) dimers is less favourable than the anti-parallel, regardless of the terminus charge. Both arrangements did not retain the extended β-sheet starting structure, but rather formed a β-hairpin-like conformation, where higher number of intermolecular interactions was made by the peptide in the anti-parallel arrangement, as discussed below. In agreement with our findings is a recent study on the effects of lipids on the dimerisation of apoC-II(60–70), where the anti-parallel orientation was determined to be more favourable than parallel.[29]

The details of the interactions between the residues were examined by constructing a residue contact map for the backbone and side-chain atoms individually, in order to determine which interactions contribute mostly to the formed structures. The contact maps shown in Fig. 6 present the backbone and side-chain distances between individual residues averaged over the structures sampled in each apoC-II(60–70) dimer trajectory.

The contact plots showed larger separations between the two monomers of the 1-2-PCh system. Clustering of close

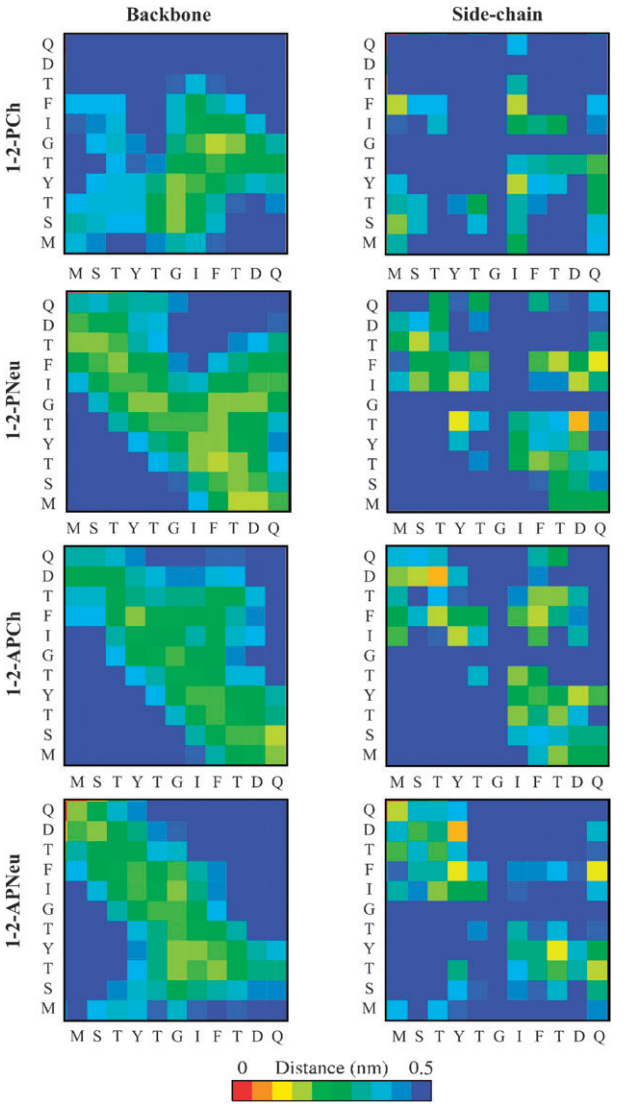

Fig. 6 Contact maps representing the average contact distance between the backbone and side-chain atoms between each residue of each dimeric system of apoC-II(60–70). The residues of monomer 1 are shown on the horizontal axis, whereas the residues of monomer 2 are shown on the vertical axis.

contacts can be seen near the central region of the two peptides, between residues Gly65 to Phe67, while the termini are not interacting strongly, exhibiting separation of more than 0.5 nm. The 1-2-PNeu system exhibited similar backbone contact distances to the 1-2-APCh and 1-2-APNeu system, where close backbone contacts between the residues can be seen in a diagonal arrangement, suggesting anti-parallel configuration. This result suggests that the (initially) parallel dimer has rearranged during the simulation to form an anti-parallel-type orientation, even though it is not in an extended β-sheet state. Interestingly, there are more close contacts seen between the backbone atoms, compared to the side-chain groups, which could suggest that in the apoC-II(60–70) dimers the backbone–backbone contacts are responsible for the β-sheet formation, while the side-chain–side-chain contacts contribute to the inter-peptide interactions and thus the fibrils

stability. Close side-chain contacts have formed between the aromatic residues, in particular in the anti-parallel system of 1-2-APCh. More recently, the role of aromatic residues in the fibril forming process and subsequent fibril stability has been shown to be significant[22] and is in line with our previous work.[13,29]

The simulations of the apoC-II(60–70) trimers exhibited similar results to the dimer systems. The least stable structures were those of the parallel oligomers, as demonstrated by the highest RMSD values (Fig. 5b). The average RMSD of the 1-3-PCh and 1-3-PNeu was 1.29 nm and 1.09 nm, respectively. In the simulation of the 1-3-PCh system, a disruption of the parallel β-strand alignment was observed by one of the external strands. Rearrangement between the strands was seen where the outer strand separated from the dimer and rotated to reattach back in an anti-parallel orientation during the equilibration stage. The structure was retained for the rest of the simulation, and can be seen in the most stable cluster of system 1-3-PCh represented in red in Fig. 5b. This result gives further insight into the possible orientation preference for fibril formation in apoC-II(60–70) peptide. Similar to our results, the transition from parallel to anti-parallel sheet has also been captured in the replica exchange studies of Jiang *et al*.[30] They demonstrated that for the transition from parallel to anti-parallel orientation a complete detachment of the strand is not required. Their results showed that the transition involved only internal reorganisation where one single hydrogen bond in the parallel pattern remained while the whole strand rotated by 180° around the hydrogen bond. Afterwards newly generated anti-parallel hydrogen bonds formed near the position of the original hydrogen bond.

The anti-parallel trimers were more stable compared to the parallel, having an average RMSD of 1.01 nm and 0.82 nm for the 1-3-APCh and 1-3-APNeu systems, respectively. A stable dimer formation can be seen in both anti-parallel trimers, having an extended β-sheet structure. The third strand of every system was found to be interacting less with the stable dimer.

The results obtained from the apoC-II(60–70) tetramer simulations exhibited in general higher structural stability in comparison to the dimer and trimer systems with the preference of anti-parallel orientation (Fig. 5c). The parallel tetramer simulations, 1-4-PCh and 1-4-PNeu, exhibited progressive instability, where the external strands were slowly starting to dissociate from the dimer. Similarly to the 1-3-PCh system (Fig. 5b), transition from parallel to anti-parallel orientation was seen to occur by one of the outer strands of the parallel tetramer. Both of these systems have charged termini, therefore in the parallel arrangement the strands are repelled from one another, then undergo reorientation into anti-parallel arrangement where they are attracted *via* the oppositely charged ends. However, even for the uncharged termini, the parallel arrangement of the apoC-II(60–70) tetramer is less stable than the anti-parallel orientation of the β-strands. The average RMSD of the parallel, 1-4-PCh and 1-4-PNeu simulations was 0.99 nm and 0.81 nm, respectively, whereas the anti-parallel, 1-4-APCh and 1-4-APNeu simulations had an average RMSD of 0.49 nm and 0.60 nm, respectively. The anti-parallel tetramers exhibited extended β-sheet conformation with high stability, represented by the high population of the most stable cluster structure shown in Fig. 5c. The average centre-of-mass separation over the entire trajectory between the four strands (1-2, 2-3, 3-4) for the 1-4-APCh system was 0.47 nm, 0.47 nm and 0.48 nm, respectively, while for the 1-4-APNeu system the average distances were 0.35 nm, 0.52 nm and 0.31 nm, respectively. These inter-strand distances correlate well with the experimentally determined values of ~0.47 nm found in most amyloid fibril structures.[31] Additional simulation of 100 ns was conducted for the anti-parallel tetramer (1-4-APCh) to identify the structure and confirm the stability of the oligomer. For this simulation only the initial velocities of the system were changed, while the starting structure was retained the same. The simulation exhibited conformations resembling those of 1-4-APCh and confirmed the stability of the oligomers structure.

Overall, our initial simulations of oligomers stability showed that an increase in the number of strands improved the stability of the oligomers dramatically, regardless of the strands orientation. However, the anti-parallel arrangement between the strands was more favourable, as indicated by the lower RMSD compared to the parallel oligomers, and the observed re-orientation of strands in some parallel systems, such as 1-2-PNeu and 1-3-PCh. This finding is in agreement with the results of our recent study on the dimerisation of apoC-II(60–70) in a lipid and lipid-free environment.[29]

Structural stabilities of mutated apoC-II(60–70) oligomers. We proceeded to investigate the effects of mutation on the structural stability of the most stable oligomer (1-4-APCh) by performing single residue substitutions at the location of Met60. The same mutations that were implemented to study the monomeric apoC-II(60–70) peptide were also applied to the oligomers: oxidised Met60 (oxi-Met), and mutations to hydrophobic Val (Met60Val) and hydrophilic Gln (Met60Gln). For clarity each system was given a name based on the mutation performed, listed in Table 1. The conformational stability of the mutated oligomers was monitored by calculating the RMSD over the entire trajectory, shown in Fig. 7. Several structures representing typical conformation observed during the simulations of the mutated systems are shown in Fig. 7.

During the 100 ns of simulation of each system the oligomers retained their β-sheet structure with some differences in their conformation. The high stability of the β-sheet structure can be attributed to the presence of strong hydrophobic core between the aromatic residues, Tyr63, Gly65, Ile66 and Phe67. Furthermore, the presence of two aromatic residues, Tyr63 and Phe67, enhanced the durability of the β-sheet by the ring π-stack formations throughout the entire trajectory of every system. The aromatic ring alignment is shown on the typical structures observed for the 1-4-APCh-oxiMet and 1-4-APCh-M60V system, depicted in Fig. 7a and b. This confirms the role of the aromatic rings in fibril formation to be significant, as discussed previously, specifically in relation to their presence in fibril forming regions and their contribution to fibril stability.[22,29]

Close inspection of Fig. 7 reveals similar trend of RMSD fluctuations between the wild-type 1-4-APCh (Fig. 5c) and 1-4-APCh-M60V systems. There was no considerable change

Table 1 System set-up listing the names given for each simulation, together with the simulation box dimensions, number of water molecules, counterions and total simulation time

System name Sheet_#strands_arrangement	Simulation box size/Å	Number of waters	Number of counterions	Simulation time/ns
Native structure oligomers				
1-2-PCh	61 × 61 × 61	7480	2 Na^+	100
1-2-PNeu	61 × 61 × 61	7487	2 Na^+	100
1-2-APCh	61 × 61 × 61	7479	2 Na^+	100
1-2-APNeu	61 × 61 × 61	7483	2 Na^+	100
1-3-PCh	63 × 63 × 63	8074	3 Na^+	100
1-3-PNeu	63 × 63 × 63	8076	3 Na^+	100
1-3-APCh	63 × 63 × 63	8069	3 Na^+	100
1-3-APNeu	63 × 63 × 63	8074	3 Na^+	100
1-4-PCh	65 × 65 × 65	8859	4 Na^+	100
1-4-PNeu	65 × 65 × 65	8850	4 Na^+	100
1-4-APCh	65 × 65 × 65	8846	4 Na^+	100
1-4-APNeu	65 × 65 × 65	8847	4 Na^+	100
Mutated oligomers				
1-4-APCh-M60Q	65 × 65 × 65	8895	4 Na^+	100
1-4-APCh-M60V	65 × 65 × 65	8899	4 Na^+	100
1-4-APCh-oxiMet	65 × 65 × 65	8894	4 Na^+	100

in the peptide arrangement or the overall structure of the oligomers in these two systems. The conformity of their typical structures can be seen in Fig. 5c and 7b. In contrast, a significant change in structure was observed in the 1-4-APCh-oxiMet and 1-4-APCh-M60Q systems, as indicated by the progressive increase in RMSD during the initial 20 ns of simulation time. Close inspection of the simulated trajectories showed a twisting motion of β-sheet structure. A typical "twisted" conformation observed for the 1-4-APCh-M60Q system is depicted in Fig. 7c. The illustration shows a central β-sheet formation with some fraying in the N- and C-termini ends. The twist and fraying at the ends can be attributed to the higher flexibility observed in the monomer studies of these mutations.

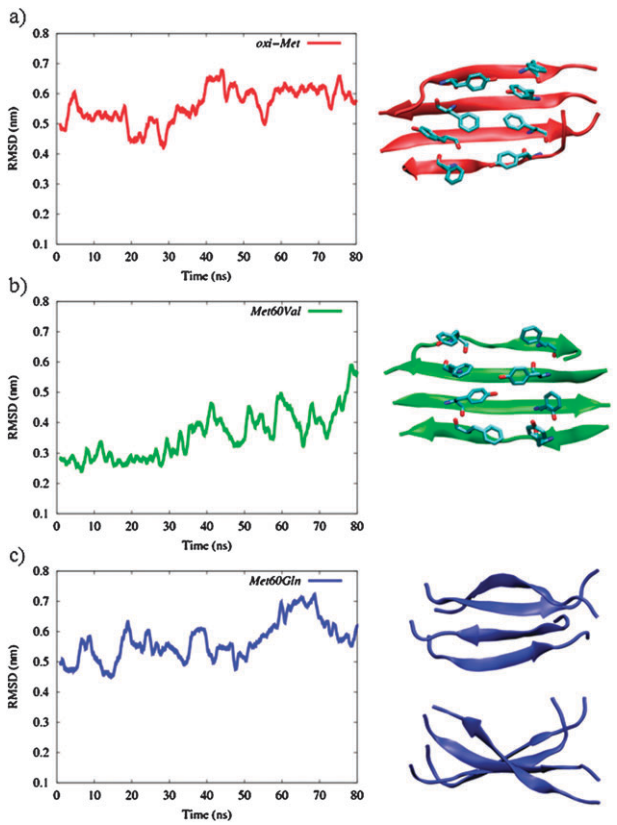

Fig. 7 Root mean square deviation (RMSD) plots of the trajectories of tetrameric apoC-II(60–70) oligomers. (a) Oxi-Met; (b) Met60Val and (c) Met60Gln. The structures of the most populated clusters of every system and their population are also presented.

Twisting in β-sheet structures has been observed for other peptides (ref. 32 and references therein). From a series of MD simulations performed under different conditions on the cross-β filament of the GNNQQNY peptide, Periole *et al*. found that in the absence of crystal packing interactions there is no free energy barrier for the twisting of the filament. Additionally, entropic contributions, in particular those associated with an increase in backbone dynamics upon twisting, stabilise the twisted form.

Overall, during the 100 ns of equilibrium simulations of each mutated system the oligomers did not dissociate and remained stable. Our simulations indicate that once the fibril nucleus has been formed, the oligomers are stable, at least in the timeframe of the current simulations which is in agreement with the ThT experiments on these peptides (Fig. 1).

Conclusions

In this study we utilised experimental and theoretical modelling techniques to determine the fibril forming propensities of the amyloidogenic apoC-II(60–70) peptide. Our results suggest that the initial structural transitions experienced by the peptide monomer are the rate-determining step for fibril formation, and MD simulations can be used to identify conformational preferences responsible for the peptide fibrillogenicity. The ThT fluorescence measurement results showed fibril formation by all peptides, however with different kinetics. The wild-type and Met60Val peptides were found to form fibrils fastest, while oxi-Met and Met60Gln peptides exhibited significantly longer lag phase.

Molecular dynamics simulations identified structural features and properties, such as the formation of a β-hairpin, higher

solvent accessible surface area and relative orientation of the aromatic side-chains, which confirmed the experimentally observed similarity between the wild-type, Met60Val and Met60Gln peptides. These features were identified as fibril-favouring for the native peptide.[13] Based on the side-chain interaction and orientation analysis performed on the two mutations Met60Val and Met60Gln we also identified some important differences, such as the broader distribution of angles observed between the aromatic Tyr63 and Phe67 residues. From entropic considerations, the most probable candidates to initiate further fibril growth are those with specific conformational structure, such as β-hairpins. Comparison of the wild-type and Met60Val systems with the oxidised and Met60Gln system revealed structural and dynamic features that can explain the observed differences in the aggregation rates. These features include increased flexibility and broader distribution of angles between the aromatic residues that were observed by the latter systems, and explain the slower rate of fibril formation.

All systems exhibited strong hydrophobic core regions, from which we can infer that the β-turn region of the peptides (Thr64, Gly65, Ile66) is a segment responsible for initiating the aggregation process, as the fibril formation is believed to be driven by the availability of the backbone atoms for hydrogen bonding and hydrophobic interactions with nearby molecules.

The computational results showed that the critical nucleus size of the apoC-II(60–70) fibrils may not be very large, since we observed that the tetrameric peptide oligomer in anti-parallel configuration is very stable within the two separate 100 ns of simulation. The termini charge had no effect on the stability and structure of the tetramer. The relatively small size of the nucleus seed of apoC-II(60–70) can explain the experimental observation of the rapid formation of amyloid fibrils, in comparison to the longer apoC-II(56–76) peptide.

The central hydrophobic core of apoC-II(60–70), between residues Tyr63 and Phe67, contributed to the stability of the tetramer. This finding was further emphasised by the stable β-sheet formation observed between these residues in the mutated apoC-II(60–70) tetramers. Oxidation and mutation of Met60 to Val and Gln did not appear to affect the stability of anti-parallel β-sheet of apoC-II(60–70). The π-stack alignment of the aromatic residues Tyr63 and Phe67 was consistent between the stable oligomers, and can be suggested to contribute to the stability of the pre-formed fibrils. This finding can explain our kinetic results which showed fibril formation by all apoC-II(60–70) peptides with different kinetics.

We have demonstrated that the effects of residue substitutions on conformation and the aggregation kinetics of shorter peptides (apoC-II(60–70) and (56–76)) differ from those observed in full-length apoC-II protein, inferring that different mechanisms can be involved in fibril formation by apoC-II and its derivative peptides.

Materials and methods

Peptide synthesis

ApoC-II(60–70) (^{60}MSTYTGIFTDQ^{70}) and derivatives mutated at position 60 were synthesised fully manually using Fmoc-solid phase peptide synthesis. Confirmation of the identity and purity (>95%) was achieved using high performance liquid chromatography (HPLC) and mass spectrometry using an LC ESI-TOF mass spectrometer (Agilent Technologies, USA). Concentrations of the stocks of the apoC-II(60–70) peptide (~20 mg ml^{-1}) in 8 M guanidine hydrochloride (GuHCl), 10 mM Tris·HCl, pH 8.0 at −20 °C were determined by measuring the absorbance at 280 nm and using a molar extinction of 1280 M^{-1} cm^{-1} at 280 nm. These stocks were stored in 8 M guanidine hydrochloride.

Thioflavin T fluorescence measurements

Fibril formation by peptides was initiated by diluting the apoC-II(60–70) stocks (as above) at room temperature into refolding buffer (0.1 M sodium phosphate, pH 7.4, 0.1% sodium azide) to a final concentration of 0.3 mg ml^{-1} for all peptides unless stated otherwise. To monitor fibril assembly, 20 μl aliquots of the peptide samples were added to 220 μl of 8 μM thioflavin T (ThT) in 0.1 M sodium phosphate, pH 7.4, 0.1% sodium azide in a single well of a 96 well plate. An f_{max} fluorescence plate reader with excitation and emission filters of 444 nm and 485 nm, respectively, was used to measure fluorescence intensities of the samples in duplicate.

Pelleting assay

The time dependent accumulation of insoluble material during the period of fibril formation by the wild-type peptide and Met60Val was followed using a pelleting assay. Fibril formation was initiated as for thioflavin T measurements. At defined points during the time course of fibril formation, 100 μl of fibril suspension was removed and centrifuged for 20 min at 100 000 rpm using a TLA 100 rotor in an OptimaMax Ultracentrifuge (Beckman Coulter, CA). 75 μl of supernatant solution was then carefully removed from the pelleted material, the absence of light scattering was confirmed and the residual concentration of soluble peptide was measured by absorbance at 280 nm. These concentrations were then used to derive the fraction of total peptide present as insoluble (pelleted) material at each time point.

Electron microscopy

Carbon coated 300-mesh copper grids (ProSciTech, Qld, Australia) were glow-discharged under partial vacuum. Following this, 4 μL aliquots of the peptide samples were diluted to 0.1 mg ml^{-1} and applied to the grid for 1 min. The grids were then washed three times with MilliQ water to remove any traces of phosphate, followed by negative staining with 1.5% (w/v) uranyl acetate. The grids were blotted with filter paper, air dried, and examined using a FEI Tecnai TF30 (Hillsborough, OR, USA). Images were taken with a Gatan US1000 2k × 2k CCD camera (Pleasanton, CA, USA) which was fitted to the TF30.

Molecular dynamics simulations

For the computational results presented in this study we employed the Gromacs 3.3[33] simulation package. The MD calculations were performed under constant pressure and temperature (NPT ensemble) conditions with the united-atom

Gromos force field parameter set 43A1.[34] Simulation conditions of constant temperature at 300 K and constant pressure of 1 bar were achieved by coupling the system to a Berendsen thermostat and barostat, respectively.[35] Long-range electrostatic interactions were calculated by the Particle Mesh Ewald (PME)[36] method with a cutoff of 10 Å for the direct space sum and a spacing of 1.2 Å for the FFT (fast Fourier transform) grid. The short-range neighbour list was cut off at 10 Å and updated every 10th step. The Lennard-Jones interactions were calculated with a cutoff of 10 Å. All bond lengths were constrained to their equilibrium value with the LINCS algorithm.[37] The time step for all the simulations was set to 2 fs.

Selected simulations were repeated with different protocol for the electrostatic interactions and Lennard-Jones cutoff to investigate if the methodology presented above overstabilises β-sheet propensities. Specifically, the simulations of valine mutated apoC-II(60–70) peptide and the tetramer in anti-parallel arrangement (most stable oligomer) were repeated with reaction field correction for the electrostatic interactions as well as Lennard-Jones cutoff of 1.4 nm. The simulations were conducted for 300 ns and 50 ns, respectively. Secondary structure evolution plots for the two systems, as well as a cartoon representation of their final structure are shown as ESI† (Fig. S1). Close inspection of the additional simulations showed that the Met60Val peptide exhibited features consistent with β-hairpin structure, while the anti-parallel tetramer experienced fraying at the terminal ends, suggesting slight instability. It can therefore be suggested that the relative differences in stability of the different structures have been robust with respect to the force field model.

Monomer simulations

The first part of our computational investigations involved the determination of the structural features exhibited by monomeric apoC-II(60–70) upon mutation. The selected starting structure for the simulations of monomeric apoC-II(60–70) was the native conformation of the 11 residue sequence (^{60}MSTYTGIFTDQ^{70}) extracted from the NMR structure of apoC-II (PDB code 1SOH). Single point mutations were performed at Met60 to Met60Val and Met60Gln, and their structural representations are shown in Fig. 8.

Each peptide was enclosed in a periodic box of 43 Å × 34 Å × 34 Å dimensions, and solvated with ~1600 SPC water molecules, corresponding to water density of ~1.0 g cm^{-3}. The whole system was energy minimised to remove steric clashes using the steepest descent approach. To allow the solvent to relax around the protein, MD equilibration was performed for 1 ns with the protein restrained. Following the equilibration stage, data collection for analysis was performed for 650 ns for each mutation.

To enable a comparison on the effects of Met60Val and Met60Gln mutations with the wild-type and oxidised apoC-II(60–70) peptide, some results from our recent publication[13] were used. In particular, the secondary structure evolution plot and aromatic angle distribution graphs are shown in Fig. 2(a and b) and 3 (red, black), respectively, together with the results obtained in this study, Fig. 2(c and d) and 3 (blue, green). Additional results obtained on the wild-type and oxi-Met apoC-II(60–70) peptides in this work, such as the most frequently sampled structures identified using an RMSD based clustering method, are shown in Fig. 2. Furthermore, calculations of the solvent accessible surface area (SASA) were performed on the structures contained within the most populated cluster of each system to allow direct comparison between the representative conformations of the wild-type and mutated peptides.

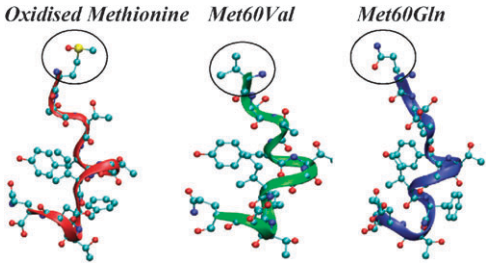

Fig. 8 Structure of apoC-II(60–70) monomeric peptide showing mutated residues used as starting conformation for the molecular dynamics simulations.

Oligomer simulations

The second part of our computational investigation involved the determination of the most stable oligomers, consisting of dimers, trimers and tetramers of the apoC-II(60–70) peptide in an extended conformation. Once the stable oligomer was identified, single point residue mutations to oxi-Met, Met60Val and Met60Gln were performed to examine their effects on the structural integrity of this oligomer.

The relative stability of pre-formed dimers, trimers and tetramers, in a single β-sheet arrangement, was investigated using classical MD. Two different strand orientations were examined, parallel (P) and anti-parallel (AP). The effect of termini charges on the stability of the formed oligomers was examined by simulating each system with charged (Ch), NH_3^+ and COO^-, and neutral (Neu), NH_2 and COOH termini ends. The extended conformation of apoC-II(60–70) peptide was chosen as the starting structure for the oligomer models because preliminary simulations on the aggregation of apoC-II(60–70) β-hairpins in various arrangements exhibited the formation of amorphous aggregates (see Fig. S2 in ESI†). This finding suggests that β-hairpin oligomers can be seen as unfavourable models for the fibril structure of apoC-II(60–70) peptide.

The oligomeric species were built with apoC-II(60–70) peptides in an extended conformation (β-strand). The strands were positioned ~0.77 nm apart from one another, thus enabling inter-strand interactions, and allowing the peptide some freedom to adopt the favoured orientations. The initial β-strand distance separation was selected to reduce the need for extensive computational sampling, but still allow the system some freedom to adopt the favoured orientations. Each oligomeric system was enclosed in a periodic cubic box with explicitly represented SPC water molecules, corresponding to water density of ~1.0 g cm^{-3} of sufficient size to eliminate oligomers self-interactions due to periodic boundary conditions. The minimum distance between periodic images was measured throughout all simulations to confirm that there

were no self-interactions. The modelled peptide–water systems had corresponding concentrations of 21.1 mg ml^{-1} (7.3 mM) for the dimer systems, 27.7 mg ml^{-1} (6.6 mM) for the trimers and 34.9 (6.0 mM) for the tetramers. The apoC-II(60–70) peptide charge of −1 was compensated by adding a Na^+ counterion for every strand present in the simulation box. Each system was simulated in an NPT ensemble for 100 ns. Table 1 shows a summary of system names, box sizes, the number of water molecules and counterions present in each simulation box, and the total simulation time for each system.

Acknowledgements

The authors would like to thank the Australian Research Council for providing funding for the project (DP0984565). The Australian National Computational Infrastructure (NCI) and Victorian Partnership for Advanced Computing (VPAC) for providing the computational resources. We also acknowledge our colleagues Sue Legge and Katrina Binger for useful discussions.

References

1 D. M. Walsh, I. Klyubin, J. V. Fadeeva, M. J. Rowan and D. J. Selkoe, *Biochem. Soc. Trans.*, 2002, **30**, 552–557.
2 N. Gosavi, H. J. Lee, J. S. Lee, S. Patel and S. J. Lee, *J. Biol. Chem.*, 2002, **277**, 48984–48992.
3 K. Sorgjerd, T. Klingstedt, M. Lindgren, K. Kagedal and P. Hammarstrom, *Biochem. Biophys. Res. Commun.*, 2008, **377**, 1072–1078.
4 K. A. Conway, S. J. Lee, J. C. Rochet, T. T. Ding, R. E. Williamson and P. T. Lansbury, Jr., *Proc. Natl. Acad. Sci. U. S. A.*, 2000, **97**, 571–576.
5 L. Hou, H. Shao, Y. Zhang, H. Li, N. K. Menon, E. B. Neuhaus, J. M. Brewer, I. J. Byeon, D. G. Ray, M. P. Vitek, T. Iwashita, R. A. Makula, A. B. Przybyla and M. G. Zagorski, *J. Am. Chem. Soc.*, 2004, **126**, 1992–2005.
6 J. M. Borreguero, B. Urbanc, N. D. Lazo, S. V. Buldyrev, D. B. Teplow and H. E. Stanley, *Proc. Natl. Acad. Sci. U. S. A.*, 2005, **102**, 6015–6020.
7 S. D. Maleknia, N. Reixach and J. N. Buxbaum, *FEBS J.*, 2006, **273**, 5400–5406.
8 L. Triguero, R. Singh and R. Prabhakar, *J. Phys. Chem. B*, 2008, **112**, 7123–7131.
9 D. M. Hatters, C. E. MacPhee, L. J. Lawrence, W. H. Sawyer and G. J. Howlett, *Biochemistry*, 2000, **39**, 8276–8283.
10 L. A. Medeiros, T. Khan, J. B. El Khoury, C. L. Pham, D. M. Hatters, G. J. Howlett, R. Lopez, K. D. O'Brien and K. J. Moore, *J. Biol. Chem.*, 2004, **279**, 10643–10648.
11 C. R. Stewart, A. Haw, 3rd, R. Lopez, T. O. McDonald, J. M. Callaghan, M. J. McConville, K. J. Moore, G. J. Howlett and K. D. O'Brien, *J. Lipid Res.*, 2007, **48**, 2162–2171.
12 K. J. Binger, M. D. W. Griffin and G. J. Howlett, *Biochemistry*, 2008, **47**, 10208–10217.
13 A. Hung, M. D. Griffin, G. J. Howlett and I. Yarovsky, *Eur. Biophys. J.*, 2008, **38**, 99–110.
14 F. S. Legge, K. J. Binger, M. D. W. Griffin, G. J. Howlett, D. Scanlon, H. Treutlein and I. Yarovsky, *J. Phys. Chem. B*, 2009, **113**, 14006–14014.
15 L. M. Wilson, Y. F. Mok, K. J. Binger, M. D. Griffin, H. D. Mertens, F. Lin, J. D. Wade, P. R. Gooley and G. J. Howlett, *J. Mol. Biol.*, 2007, **366**, 1639–1651.
16 V. Knecht, *J. Phys. Chem. B*, 2008, **112**, 9476–9483.
17 G. Wei and J. E. Shea, *Biophys. J.*, 2006, **91**, 1638–1647.
18 M. Nishino, Y. Sugita, T. Yoda and Y. Okamoto, *FEBS Lett.*, 2005, **579**, 5425–5429.
19 M. D. W. Griffin, M. L. Y. Mok, L. M. Wilson, C. L. L. Pham, L. J. Waddington, M. A. Perugini and G. J. Howlett, *J. Mol. Biol.*, 2008, **375**, 240–256.
20 D. Frishman and P. Argos, *Proteins: Struct., Funct., Genet.*, 1995, **23**, 566–579.
21 F. S. Legge, H. Treutlein, G. J. Howlett and I. Yarovsky, *Biophys. Chem.*, 2007, **130**, 102–113.
22 E. Gazit, *FEBS J.*, 2005, **272**, 5971–5978.
23 R. Azriel and E. Gazit, *J. Biol. Chem.*, 2001, **276**, 34156–34161.
24 C. Wu, H. Lei and Y. Duan, *Biophys. J.*, 2005, **88**, 2897–2906.
25 A. Fernandez and H. A. Scheraga, *Proc. Natl. Acad. Sci. U. S. A.*, 2003, **100**, 113–118.
26 B. Ma and R. Nussinov, *Proc. Natl. Acad. Sci. U. S. A.*, 2002, **99**, 14126–14131.
27 M. F. Masman, U. L. Eisel, I. G. Csizmadia, B. Penke, R. D. Enriz, S. J. Marrink and P. G. Luiten, *J. Phys. Chem. B*, 2009, **113**, 11710–11719.
28 A. Melquiond, N. Mousseau and P. Derreumaux, *Proteins: Struct., Funct., Bioinf.*, 2006, **65**, 180–191.
29 A. Hung, M. D. W. Griffin, G. J. Howlett and I. Yarovsky, *J. Phys. Chem. B*, 2009, **113**, 9447.
30 P. Jiang, W. Xu and Y. Mu, *PLoS Comput. Biol.*, 2009, **5**, e1000357.
31 M. R. Sawaya, S. Sambashivan, R. Nelson, M. I. Ivanova, S. A. Sievers, M. I. Apostol, M. J. Thompson, M. Balbirnie, J. J. W. Wiltzius, H. T. McFarlane, A. O. Madsen, C. Riekel and D. Eisenberg, *Nature*, 2007, **447**, 453–457.
32 X. Periole, A. Rampioni, M. Vendruscolo and A. E. Mark, *J. Phys. Chem. B*, 2009, **113**, 1728–1737.
33 D. van der Spoel, E. Lindahl, B. Hess, G. Groenhof, A. E. Mark and H. J. C. Berendsen, *J. Comput. Chem.*, 2005, **26**, 1701–1718.
34 W. F. van Gunsteren, S. R. Billeter, A. A. Eising, P. H. Hunenberger, P. Kruger, A. E. Mark, W. R. P. Scott and I. G. Tironi, *Biomolecular Simulation: The GROMOS96 Manual and User Guide*, ETH Zurich and BIOMOS b.v, Zurich, Groningen, 1996.
35 H. J. C. Berendsen, J. P. M. Postma, W. F. van Gunsteren, A. Dinola and J. R. Haak, *J. Chem. Phys.*, 1984, **81**, 3684–3690.
36 T. E. Cheatham, J. L. Miller, T. Fox, T. A. Darden and P. A. Kollman, *J. Am. Chem. Soc.*, 1995, **117**, 4193–4194.
37 B. Hess, H. Bekker, H. J. C. Berendsen and J. G. E. M. Fraaije, *J. Comput. Chem.*, 1997, **18**, 1463–1472.

